Design of a Carbonic Anhydrase IX Active-Site Mimic To Screen Inhibitors for Possible Anticancer Properties[†,‡]

Caroli Genis,[§] Katherine H. Sippel,[§] Nicolette Case,[§] Wengang Cao,[||] Balendu Sankara Avvaru,[§] Lawrence J. Tartaglia,[§] Lakshmanan Govindasamy,[§] Chingkuang Tu,[⊥] Mavis Agbandje-McKenna,[§] David N. Silverman,[§,⊥] Charles J. Rosser,[||] and Robert McKenna*[,§]

Department of Biochemistry and Molecular Biology, Department of Urology, and Department of Pharmacology and Therapeutics, College of Medicine, University of Florida, Gainesville, Florida 32610

Received October 31, 2008; Revised Manuscript Received December 17, 2008

ABSTRACT: Recently, a convincing body of evidence has accumulated suggesting that the overexpression of carbonic anhydrase isozyme IX (CA IX) in some cancers contributes to the acidification of the extracellular matrix, which in turn promotes the growth and metastasis of the tumor. These observations have made CA IX an attractive drug target for the selective treatment of certain cancers. Currently, there is no available X-ray crystal structure of CA IX, and this lack of availability has hampered the rational design of selective CA IX inhibitors. In light of these observations and on the basis of structural alignment homology, using the crystal structure of carbonic anhydrase II (CA II) and the sequence of CA IX, a double mutant of CA II with Ala65 replaced by Ser and Asn67 replaced by Gln has been constructed to resemble the active site of CA IX. This CA IX mimic has been characterized kinetically using ^{18}O-exchange and structurally using X-ray crystallography, alone and in complex with five CA sulfonamide-based inhibitors (acetazolamide, benzolamide, chlorzolamide, ethoxzolamide, and methazolamide), and compared to CA II. This structural information has been evaluated by both inhibition studies and in vitro cytotoxicity assays and shows a correlated structure−activity relationship. Kinetic and structural studies of CA II and CA IX mimic reveal chlorzolamide to be a more potent inhibitor of CA IX, inducing an active-site conformational change upon binding. Additionally, chlorzolamide appears to be cytotoxic to prostate cancer cells. This preliminary study demonstrates that the CA IX mimic may provide a useful model to design more isozyme-specific CA IX inhibitors, which may lead to development of new therapeutic treatments of some cancers.

Carbonic anhydrases (CAs)[1] are zinc−metalloenzymes that catalyze the reversible interconversion of CO_2 and HCO_3^- (*1*). Since their discovery, the CAs have been extensively studied due to their important physiological functions in all kingdoms of life. This family of enzymes is broadly composed of three well-studied, structurally distinct (α, *β*, and *γ*) classes. The α-class is present in vertebrates but is also shown to be present in other organisms. They (and α-CA domains in more complex isoforms) have a molecular weight of ∼29 kDa. There are 14 expressed α-CAs (CA I−XIV) in humans, and the active CAs play roles in respiration, pH homeostasis, fluid production, and other functions as yet to be determined (*2*−*5*). The α-CAs all share the same overall mixed α/*β* fold with approximate dimensions of 50 × 40 × 40 Å^3. The active site is characterized by a conical cavity that is approximately 15 Å deep. The zinc ion is located at the bottom of the conical active-site cavity and is tetrahedrally coordinated by three histidine ligands and a bound hydroxide/water (*1*). The active sites between isoforms are nearly identical, other than a few amino acids that line the cavity (*6*).

Carbonic anhydrase IX (CA IX) is a unique member of the human α-class of CAs, as it is a membrane-associated glycoprotein, composed of several domains including a short intracellular region, a single transmembrane helix, and an extracellular proteoglycan domain as well as a catalytic CA domain (*7*). Under normal conditions, CA IX is commonly expressed in cells that are thought to need to maintain extracellular pH, such as gastric mucosal cells. However, in many cancers it is overexpressed as a result of hypoxia (*3*). The regulation of the CA IX gene has been shown to be controlled by hypoxia inducing factor-1 (*7*). It has been hypothesized that as tumor growth progresses and becomes

[†] This work was supported by a grant (GM25154 to D.N.S. and R.M.) from the National Institutes of Health and the Maren Foundation (to R.M.).

[‡] Coordinates and structure factors have been deposited in the Protein Data Bank as 3DC9.pdb and 3DC9.sf, 3DCS.pdb and 3DCS.sf, 3DCC.pdb and 3DCC.sf, 3DC3.pdb and 3DC3.sf, 3DCW.pdb and 3DCW.sf, 3DBU.pdb and 3DBU.sf, 3DAZ.pdb and 3DAZ.sf, 3D9Z.pdb and 3D9Z.sf, 3DD0.pdb and 3DD0.sf, and 3D8W.pdb and 3D8W.sf.

* To whom correspondence should be addressed. Telephone: (352) 392-5696. Fax: (352) 392-3422. E-mail: rmckenna@ufl.edu.

[§] Department of Biochemistry and Molecular Biology.

[||] Department of Urology.

[⊥] Department of Pharmacology and Therapeutics.

[1] Abbreviations: CAs, carbonic anhydrases; CA II, carbonic anhydrase II; CA IX, carbonic anhydrase IX; CA IX mimic, double mutant of CA II with Ala65 replaced by Ser and Asn67 replace by Gln to resemble the active site of CA IX; AZM, acetazolamide; BZM, benzolamide; CHL, chlorzolamide; EZM, ethoxzolamide; MZM, methazolamide; CGLS, conjugate-gradient least-squares; K_i, inhibition constant.

10.1021/bi802035f CCC: $40.75
Published on Web 01/26/2009

insufficient to maintain a supply of oxygen, the cancer cell remodels metabolically, which is partially achieved by the up-regulation of CA IX. Therefore, CA IX is considered to be a marker of tumor hypoxia (*8*).

In hypoxic tumors, it is believed that CA IX plays a critical role in cell survival. In tumors there is an observed increase in CO_2 concentration (*9, 10*). It is believed that this is not a result of oxidative metabolism but rather a byproduct of an increase in the pentose phosphate pathway. This serves to replenish the supply of NADPH and generate ribose-5-phosphate, necessary for nucleotide and coenzyme production (*11*). The surplus of CO_2 is converted to HCO_3^- and a proton by CA IX, creating the significant increase in extracellular proton concentration causing the acidification of the tumor microenvironment. The alteration in proton flux is also believed to affect the activity of ion transporters and channels (*5*). Additionally, the acidity may cause the exclusion of weakly basic chemotherapeutic agents rendering traditional therapies less effective (*7*). The proteoglycan domain of CA IX has been implicated in the disruption of cell−cell adhesion by breaking the connection of E-cadherin to the cytoskeleton, which may lead to tumor invasion (*12*). Several studies have shown that inhibition of CA IX can lead to decreased invasiveness, as well as inducing cell death under hypoxic conditions (*3, 8, 13*−*16*). These factors, taken together, provide strong evidence to suggest that CA IX might be an attractive drug target for the treatment of cancers.

One significant barrier that needs to be overcome for the development of CA IX inhibitors as effective cancer treatments is to produce a CA IX isoform-specific inhibitor, which has a significantly higher affinity for CA IX than other active CA isoforms. The development of a high-affinity CA IX inhibitor has been hampered due to the lack of an available crystal structure of CA IX. CA IX is a membrane protein and has so far proven itself difficult to express in sufficient soluble and properly folded quantities for crystallization (*17, 18*). To overcome these issues, this research reports the expression and structural and kinetics studies of a CA IX active-site mimic. The design of the CA IX mimic is based on a structural-alignment comparison with CA II and is a double mutant of CA II (A65S-N67Q CA II) that imitates the active site of CA IX. This CA IX mimic was expressed and characterized both kinetically and crystallographically, by itself and in complex with several common sulfonamide inhibitors, acetazolamide (AZM), benzolamide (BZM), chlorzolamide (CHL), ethoxzolamide (EZM), and methazolamide (MZM). Preliminary data reveal that the inhibition profiles of the CA IX mimic mirror wild-type CA IX compared to values previously published (*17*). In addition, the crystal structures of the CA IX mimic bound to these drugs reflect the kinetics, showing chlorzolamide as the drug with greatest affinity to CA IX, and the CA IX mimic undergoes active-site conformational changes rather than a simple lock and key model of inhibition. Further, this structural information has been evaluated in relationship to inhibition studies and in vitro cytotoxicity assays and shows a correlated structure−activity relationship. To our knowledge, this is the first time a protein mimic has been engineered from a related isozyme for the purpose of drug design. The CA IX mimic presented provides a unique opportunity in developing and assessing CA IX isoform-specific inhibitors, while ongoing studies attempt to obtain the crystal structure of the catalytic domain of CA IX.

MATERIALS AND METHODS

In Silico Design of the CA IX Mimic. All 14 human CA sequences were obtained from the NCBI database and a multiple sequence alignment was performed using Clustal W (*19*). A CA IX model was built with the Swiss-Model, using the high resolution CA II crystal structure (PDB accession code: 2ILI) as a template (*20, 21*). The molecular graphics programs Coot was used to visualize and analyze the CA IX model (*22*).

Enzyme Expression and Purification. The CA IX mimic was made by site-directed mutagenesis using an expression vector containing the CA II coding region (*23, 24*). Residues Ala65 and Asn67 were mutated to Ser and Gln, respectively. Site-directed mutagenesis was accomplished using the Quick Change Mutagenesis kit from Stratagene using CA II as a template and the primers (mutations in bold): 5′-CCTCAACAATGGTCAT**TC**G**T**TC**CA**G**G**TGGAGTTTGATGAC-3′ and 5′-GTCATCAAACTCCAC**CTG**GAA**C**GA**A**ATGACCATTGTTGAGG. The DNA sequence was confirmed for the entire coding region for the CA in the expression vector. Expression of the CA IX mimic vector was done by transforming into *Escherichia coli* BL21(DE3)pLysS, which does not express any endogenous α-CA (*25, 26*). The purification of CA IX mimic and CA II was performed on an affinity column of *p*-amino-methyl-benzenesulfonamide, as described previously in ref (*27*). The protein was collected, then buffer exchanged into 50 mM Tris−HCl, pH 7.8, concentrated, and then analyzed for expression and purity using Coomassie-stained SDS-PAGE. The final protein concentration was ∼15 mg mL^{-1} as calculated by measuring the optical density at 280 nm using a molar absorptivity of 5.5×10^4 M^{-1} cm^{-1}.

Crystallization. Crystals of CA II and CA IX mimic were grown at room temperature using the hanging-drop vapor-diffusion method (*28*). Crystallization drops were prepared by mixing 7 μL protein (∼15 mg mL^{-1} in 50 mM Tris−HCl, pH 7.8) with 3 μL precipitant solution (100 mM Tris−HCl, pH 9.0, 1.3 M sodium citrate) and 1 μL of Hampton HR2-410-02 detergent (Hampton Research, Aliso Viejo, CA). The hanging-drops were equilibrated against 1 mL precipitant solution. Crystals appeared within 5 days.

Drug Soaks. The CA inhibitors (acetazolamide (AZM), benzolamide (BZM), chlorzolamide (CHL), ethoxzolamide (EZM), and methazolamide (MZM) see Table 1) were solubilized in water, with AZM, CHL, and MZM requiring the addition of 50%, 10%, and 5% of DMSO, respectively. CA IX mimic and CA II crystals were incubated with the inhibitor solutions at 4 mM final concentration for ∼24 h prior to X-ray diffraction data collection. As the density for DMSO is not found in any of the structures presented and the density of the drugs are continuous, it is assumed that the high concentration of DMSO in the drug soaks is not affecting either binding or the chemical composition of these molecules.

Diffraction Data Collection. All the diffraction data for both the CA IX mimic and CA II crystals were collected "in-house" on the RAXIS IV^{++} detector using Cu K_α

Table 1: Carbonic Anhydrase Inhibitors[a]

AZM)

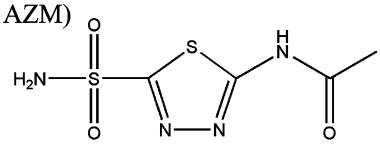

BZM)

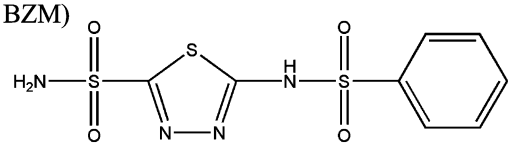

CHL)

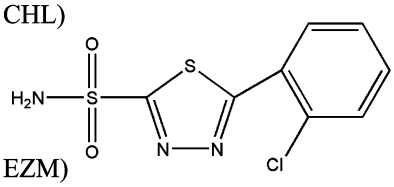

EZM)

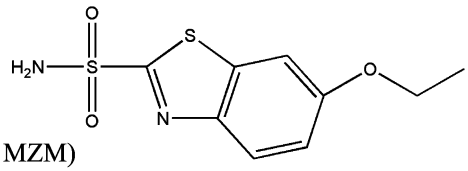

MZM)

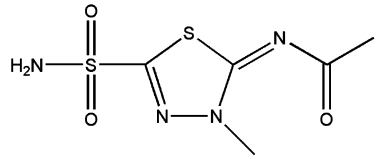

[a] AZM, acetazolamide (*N*-(5-(aminosulfonyl)-1,3,4-thiadiazol-2-yl)-acetamide); BZM, benzolamide (1,3,4-thiadiazole-2-sulfonamide,5-((phenylsulfonyl)amino); CHL, chlorzolamide (5-[*o*-chlorophenyl]-1,3,4-thiadiazole-2-sulfonamide); EZM, ethoxzolamide (6-ethoxybenzothiazole-2-sulfonamide); MZM, methazolamide (*N*-(3-methyl-5-sulfamoyl-3*H*-1,3,4-thiadiazol-2-ylidene).

wavelength (1.5418 Å). The crystal-to-detector distance was set at a range of 80−100 mm (dependent on the quality of diffraction) and images were collected in one degree oscillation steps with a 300 s exposure time. The data were merged using *DENZO* and scaled with *SCALEPACK* using HKL 2000 (*29*). Data statistics are listed in Tables 2 and 3.

Structure Determination. All the crystal structures were determined by molecular replacement methods using the previously solved wild-type CA II structure with solvents removed (PDB code 2ILI) (*20*). Initially, the structures were refined using the standard refinement protocol of CNS program version 1.1, which included rigid-body, *B*-factor and energy minimization (*30*). Difference Fourier maps provided clear, phase-unbiased electron density for the respective bound inhibitors. The PRODRG server was used to generate topology files for modeling the inhibitor structures during the subsequent refinement process (*31*). Once the inhibitors were modeled using the program COOT, refinement continued using the program SHELXL97 (*22, 32*). The conjugate-gradient least-squares model (CGLS) with SHELXL default restraints were used for the protein geometric parameters followed by manual model building with the computer-graphics program COOT and the addition of solvent molecules (*22, 32*). Refinement of the structures continued until the R_{cryst} and R_{free} converged. The inhibitor-enzyme interactions were determined by observing environmental distances in COOT and the model geometries were analyzed using *PROCHECK* (*22, 33*). The coordinates and structure factors for all nine structures have been submitted to the Protein Data Bank. PDB files, data-refinement, and final model statistics are given in Tables 2 and 3.

Oxygen-18 Isotope Exchange Kinetic and Inhibition Studies. Inhibition constants (K_i values) of all compounds were determined by the measurement of the inhibition of the ^{18}O-exchange activity between CO_2 and water via mass spectrometry, as reviewed elsewhere (*34, 35*). Experiments were carried out at 25 °C in solutions buffered at pH 7.4 with 0.1 M HEPES. The concentration of all species of carbonate was 10 mM, 93% HCO_3^-, 7% CO_2, and 0.1% CO_3^{2-}. The enzyme concentration was 7.3 nM. Inhibitor concentrations went up to 800 μM and were analyzed by the method of Henderson for tight-binding inhibitors (*36*).

Cell Lines and Culture. Human prostate cancer cell line PC-3-*Bcl*-2 (characterized by marked *Bcl*-2 overexpression, PTEN deletion, and p53 mutation) was a generous gift from Dr. Timothy McDonnell (The University of Texas M. D. Anderson Cancer Center, Houston, TX). These cells were maintained in Dulbecco's modified Eagle's medium (Mediatech, Inc., Herndon, VA) with 4.5 g/L glucose, 4 mM L-glutamine, 10% fetal bovine serum, 100 units/mL penicillin, 100 μg/mL streptomycin, and 500 μg/mL G418. All cells were incubated at 37 °C in a humidified atmosphere of 5% CO_2 in air.

In Vitro Cytotoxicity Assay. The prostate cancer cell line stably transfected to overexpress *Bcl*-2. PC-3-*Bcl*-2 cells were seeded in 96-well plates at a density of 2.5×10^3 cells per well and treated with drug, control (DMSO only), or mock. The CA inhibitors were dissolved in DMSO and administered at concentrations ranging from 0 to 100 000 nM. After 1−4 days, 100 μL of 1 mg/mL MTT (Sigma-Aldrich, St. Louis, MO) solution was added to appropriate plates and allowed to incubate at 37 °C for 2.5 h (*37*). Each reaction was stopped with lysis buffer (200 mg/mL SDS, 50% *N*,*N*-dimethylformamide, pH 4) at room temperature for 1 h, and the optical density was read on a microplate autoreader (Bio-Tek Instruments, Winooski, VT) at 560 nm. Absorbance values were normalized to the values obtained for the mock treated cells to determine survival percentages. Each assay was performed in triplicate, and the mean was calculated from these three assays. Cellular viability was confirmed by means of the crystal violet exclusion test (*37*).

Western Blot Analysis. For protein extraction, cells were lysed in lysis buffer [250 mM Tris−HCl (pH 6.8), 2% SDS, and 10% glycerol] and protein inhibitor cocktail (Sigma, St. Louis, MO). A standard protein assay was performed using the DC Protein Assay kit (Bio-Rad, Hercules, CA). Western blot analysis was completed as described previously in ref (*38*). Immunoblotting was performed by first incubating the proteins with primary antibodies against CA IX (Novus Biologicals, Littleton, CO) and γ-tubulin (Santa Cruz Biotechnology, Santa Cruz, CA), and then with HRP-conjugated secondary antibody (Bio-Rad). Protein antibody complexes were detected by means of chemiluminescence (Amersham, Arlington Heights, IL).

RESULTS

Sequence and Structural Alignment Comparison. The multiple-sequence alignment showed the extracellular CA-

Table 2: Crystallographic Statistics for CA IX Mimic Alone and in Complex

data set statistics	no drug	MZM	CHL	AZM	EZM	BZM
space group	$P2_1$	$P2_1$	$P2_1$	$P2_1$	$P2_1$	$P2_1$
unit-cell parameters						
a (Å)	42.8	42.9	42.9	42.9	42.8	42.8
b (Å)	41.8	41.8	41.9	41.8	41.7	42.0
c (Å)	72.8	73.0	73.0	72.9	72.8	72.7
β (deg)	104.5	104.6	104.6	104.5	104.5	104.4
resolution (Å)	20−1.60 (1.66−1.60)	20−1.80 (1.86−1.80)	20−1.60 (1.66−1.60)	20−1.70 (1.76−1.70)	20−1.50 (1.55−1.50)	20−1.70 (1.76−1.70)
total number of reflections	92791	62807	56620	82430	140381	99710
unique reflections	31389 (3000)	22064 (2141)	26650 (2547)	26697 (2573)	37113 (3476)	25878 (2472)
redundancy	3.0	2.8	2.1	3.1	3.8	3.9
completeness (%)	94.9 (91.4)	93.8 (91.1)	79.8 (76.5)	96.0 (93.4)	92.3 (87.2)	93.1 (89.2)
R_{sym}	0.074 (0.279)	0.101 (0.328)	0.064 (0.297)	0.068 (0.311)	0.081 (0.430)	0.089 (0.488)
refinement statistics						
$R_{factor}{}^a/R_{free}{}^b$	0.151/0.200	0.145/0.214	0.146/0.206	0.141/0.193	0.155/0.190	0.143/0.197
rmsd for bond lengths/angles (deg)	0.008/0.026	0.006/0.022	0.008/0.024	0.007/0.024	0.009/0.026	0.007/0.023
average B-factors (Å^2)						
no. protein atoms	2082	2081	2110	2110	2122	2128
main/side/solvent	15.6/23.6/29.1	16.1/23.8/27.1	15.7/23.0/28.7	17.3/24.6/37.5	18.6/25.5/29.8	19.8/27.1/29.3
no. water molecules	188	165	180	174	170	163
drug	N/A	16.0	16.4	17.8	22.5	32.1
Ramachandran statistics (%)						
most favored	88.4	88.0	87.0	90.7	88.9	86.6
additional & generously	11.6	12.0	13.0	9.3	10.6	13.0
allowed/disallowed	0/0	0/0	0/0	0/0	0.5/0	0.5/0
PDB-ID	3DC9	3DCS	3DCC	3DC3	3DCW	3DBU

[a] $R_{factor} = \sum||F_{obs}| - |F_{calc}||/\sum|F_{obs}|$. [b] R_{free} was monitored using 5% of the reflection data excluded from refinement.

Table 3: Crystallographic Statistics for CA II-Complexed Structures

data set statistics	MZM	CHL	EZM	BZM
space group	$P2_1$	$P2_1$	$P2_1$	$P2_1$
unit-cell parameters				
a (Å)	42.8	42.9	42.8	42.8
b (Å)	41.7	41.8	41.7	42.1
c (Å)	72.9	72.9	72.9	72.7
β (deg)	104.6	104.6	104.6	104.6
resolution (Å)	20−1.60 (1.66−1.60)	20−1.65 (1.71−1.65)	50−1.48 (1.53−1.48)	20−1.70 (1.76−1.70)
total number of reflections	88307	65568	112975	73979
unique reflections	32589 (3179)	28166 (2674)	39340 (3727)	26998 (2596)
redundancy	2.7	2.3	2.9	2.7
completeness (%)	98.3 (96.3)	93.0 (89.2)	94.2 (89.3)	96.7 (94.1)
R_{sym}	0.067 (0.358)	0.055 (0.393)	0.057 (0.214)	0.067 (0.323)
refinement statistics				
$R_{factor}{}^a/R_{free}{}^b$	0.148/0.197	0.145/0.190	0.149/0.180	0.146/0.195
rmsd for bond lengths (Å)/ angles (deg)	0.006/0.025	0.007/0.024	0.011/0.027	0.007/0.023
average B-factors (Å^2)				
no. protein atoms	2104	2064	2073	2068
main/side/solvent	17.3/24.8/29.9	15.5/23.7/28.2	16.2/23.3/32.3	18.9/26.0/29.8
no. water molecules	182	184	206	175
drug	18.2	16.0	13.6	27.5
Ramachandran statistics (%)				
most favored	88.4	88.0	87.6	88.0
additional and generously	11.6	12.0	12.0	11.6
allowed/disallowed	0/0	0/0	0.5/0	0.5/0
PDB-ID	3DAZ	3D9Z	3DD0	3D8W

[a] $R_{factor} = \sum||F_{obs}| - |F_{calc}||/\sum|F_{obs}|$. [b] R_{free} was monitored using 5% of the reflection data excluded from refinement.

domain of CA IX (residues 141−390) shared a 39% sequence identity with CA II (residues 1−261). This variation in sequence is approximately the average value of sequence conservation among the human CAs. Superimposition of the three-dimensional Swiss-Model of the catalytic domain of CA IX onto CA II gave an rmsd of the Cα atoms of 0.6 Å. Not surprising, most of the amino-acid differences between the two isoforms were on the surface. The three centrally located histidines (residues H94, H96, and H119 in the CA II numbering) that coordinate the zinc ion, the second sphere residues that coordinate the histidines (Q92, S117, and the carbonyl of residue 244), and the amino acids that form the hydrophobic CO_2 binding pocket (residues V121, V143, L198, T199-CH_3, V207 and W209 in the CA II numbering). were completely conserved (Figure 1). Having a 15 Å diameter entrance that tapers into the center of the enzyme, the active-site cavity of CA II can be loosely described as being conical in shape. This cavity is lined with hydrophilic amino acids (residues Y7, N62, H64, A65, N67, T199-Oγ_1 and T200-Oγ_1 in the CA II numbering), and these residues exhibit variation between different isoforms. These amino acids are believed to create a solvent network that influences the rate-limiting proton-transfer step in catalysis. On close inspection of the active-site cavity model of CA IX, it differed from CA II with respect to two of these amino acids, namely, A65S and N67Q (based on CA II residue number-

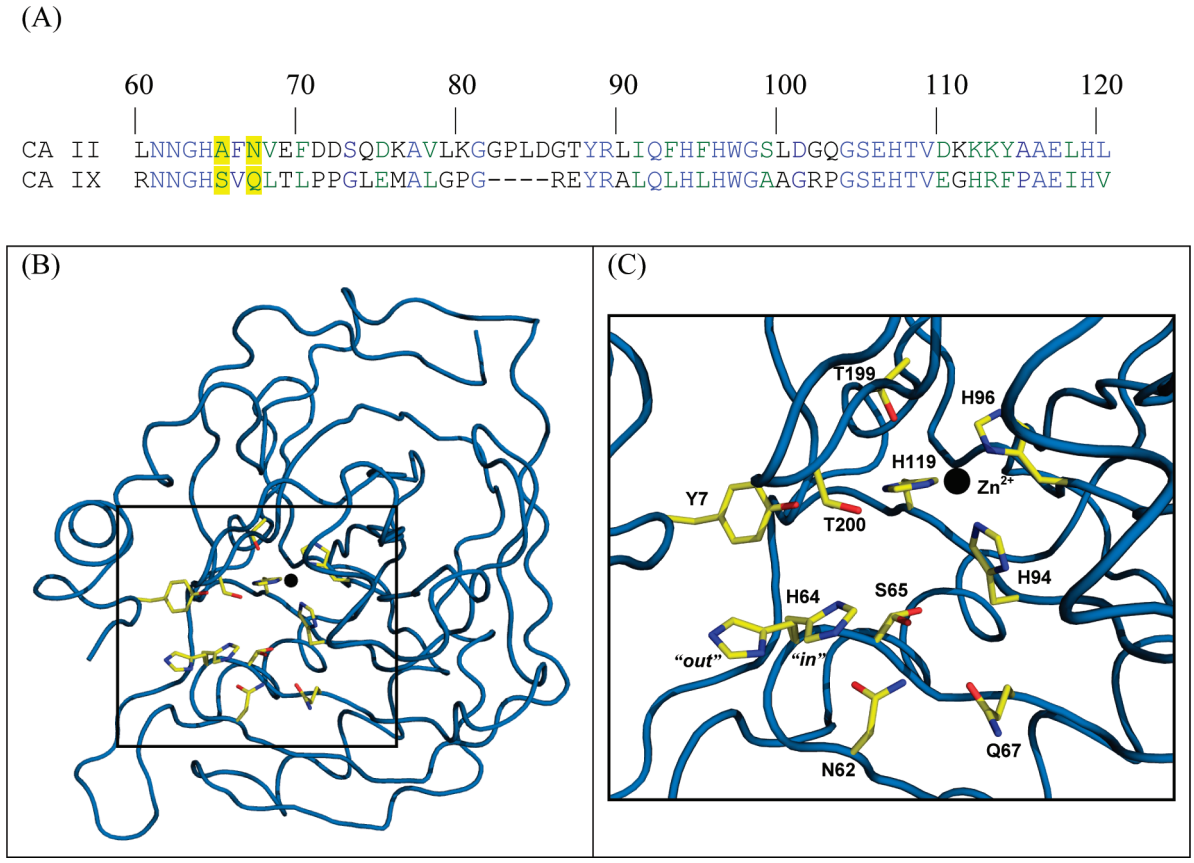

FIGURE 1: Sequence and structure of unbound CA IX mimic. (A) Amino acid sequence alignment of CA II and CA IX from residue 60 to 120 (CA II numbering). Conserved residues His64, His94, His96, His119, and all active-site residues are colored blue. Active-site variants, residues 65 and 67, are highlighted in yellow. Alignment performed using Clustal W (*19*). (B) Crystal structure of CA IX mimic. Backbone (blue cartoon), active-site residues (yellow sticks as labeled), Zn^{2+} (black sphere). (C) Close up view of CA IX mimic. Figure B was generated and rendered in PyMOL (*43*).

ing) (Figure 1a). It was hypothesized that these two amino acid differences could cause variations in binding affinity of small molecule inhibitors. Therefore, these point mutations were made to CA II to create the CA IX mimic. It is of note that there is an Ala65 in many CAs; in CA II from mouse, rat, and chicken; in CA VII; and in some CA IV's. There is a Gln67 in CA V; CA VI; CA VII; and in α-CA from *Neisseria* and *Chlamydomonas*; and in CA VIII.

Kinetic Comparison. Duda et al. have previously reported the pH profile of k_{cat}/K_m for CO_2 hydration and the proton-transfer-dependent rate constant (R_{H_2O}) derived from ^{18}O exchange for CA II with a k_{cat}/K_m for CO_2 hydration of (9.8 ± 5) × 10^7 $M^{-1}s^{-1}$ and a maximal rate constant for proton transfer from the donor to zinc-bound hydroxide of (8.0 ± 1) × 10^5 (*39*). Similarly, the catalytic domain (residues 141−390) of CA IX has been previously cloned and kinetically characterized (*17*). The pH profile of k_{cat}/K_m for CO_2 hydration was derived from ^{18}O exchange data and was described by a single ionization with an apparent pK_a of 6.3, with a maximal k_{cat}/K_m of (5.5 ± 0.1) × 10^7 M^{-1} s^{-1}. In addition, the pH profile for the proton-transfer-dependent rate constant of CA IX (R_{H_2O}) was shown to be bell-shaped at pH 5−8, similar to CA II with R_{H_2O} corresponding to a rate-limiting proton transfer from a donor of pK_a 6.4 to an acceptor (zinc-bound hydroxide) with a pK_a of 6.4. This was consistent with the pK_a obtained from the pH profile of k_{cat}/K_m for CO_2 hydration. The maximal rate constant for proton transfer from the donor to zinc-bound hydroxide was (1.4 ± 0.3) × 10^6 s^{-1}.

Table 4: K_i Values (nM) of Inhibitors for CA II, CA IX Mimic and CA IX

inhibitor	CA II	CA IX mimic	wild-type CA IX
AZM	10.1 ± 0.7	4.9 ± 1	3.0[a]
BZM	7.0 ± 0.9	8.8 ± 1.2	9.0 ± 1.0
EZM	<1	<1	
CHL	2.0 ± 0.4	1.1 ± 0.2	1.0 ± 0.3
MZM	11.8 ± 1.8	11.4 ± 2	9.0[a]

[a] Data from ref (*17*).

Similarly, to compare the kinetic properties of CA II and wild-type CA IX to the CA IX mimic, the same ^{18}O protocols were employed. The pH profile (data not shown) determining the k_{cat}/K_m (M^{-1} s^{-1}) for hydration of CO_2 catalyzed by CA IX mimic was (5.1 ± 0.2) × 10^7 $M^{-1}s^{-1}$ with a $(pK_a)_{ZnH_2O}$ of 6.7 ± 0.1, and the pH profile for the proton-transfer-dependent rate constant was fitted and determined to be (8.2 ± 1) × 10^5 s^{-1}, $(pK_a)_{donor}$ = 6.8 ± 0.1 and $(pK_a)_{ZnH_2O}$ = 5.7 ± 0.1. These data were obtained at 25 °C in the absence of buffer using a total concentration of all CO_2 species of 25 mM with the ionic strength maintained at 0.2 M by the addition of sodium sulfate.

Drug Inhibition Studies. Oxygen-18 exchange methods were also used to measure the inhibition of CA II and the CA IX mimic with the inhibitors AZM, BZM, CHL, EZM, and MZM (Table 1) and compared to available values for CA IX (*17*). The values measured are given in Table 4. Assessment of the isozyme specificity reveals that AZM, the benchmark CA inhibitor, exhibited a 2−3-fold better binding

affinity for CA IX to CA II, with a K_i of 3.0 nM for wild-type CA IX, 4.9 nM for the CA IX mimic, and 10.1 nM for CA II. This result further demonstrated that the CA IX mimic was more like CA IX than CA II. Of additional interest was that CHL exhibited the highest measurable binding affinity of the four inhibitors with accurate data to determine a K_i. It has a K_i of 1.1 nM for the CA IX mimic, approximately 2-fold better than the K_i of 2.0 nM for CA II. The inhibitors BZM and MZM showed no significant preferential binding to the CA IX mimic compared to CA II, though BZM was the more potent inhibitor overall, and EZM was a subnanomolar inhibitor below the sensitivity of the Oxygen-18 exchange method instrumentation. This made it impossible to accurately measure the K_i of EZM in these studies.

Crystallographic Study. A complete structural comparison of the binding profiles of the five CA inhibitors (Table 1) was performed with both CA II and the CA IX mimic. All the inhibitor-soaked crystals were isomorphous to each other, in the monoclinic space group $P2_1$, with mean unit cell dimensions: $a = 42.8 \pm 0.1$ Å, $b = 41.8 \pm 0.1$ Å, $c = 72.9 \pm 0.1$ Å, and $\beta = 104.5 \pm 0.1°$. The initial electron-density-omit maps showed unambiguously all the inhibitors had bound in the active-site cavity (Figure 2). This binding site has been well characterized for CA II and other α-CA isoforms (*1*). All the structures had expected refinement statistics for structures at 1.5−1.8 Å resolution with comparable *R* factors and rmsd values to CA II (Tables 3 and 4). A summary for each of the inhibitor's interactions with CA II and CA IX are listed in Table 5. Hydrogen bonds and hydrophobic contact distances that change 0.2 Å or less fall within refinement error and are considered to be the same. The unbound CA IX mimic structure had an rmsd value for 249 Cα atoms of 0.23 Å compared to CA II (PDB code 2ILI) (*20*). There were no significant conformational changes between the unbound CA II and the CA IX mimic, with the exception of residue Ser65 of CA IX mimic exhibited a dual conformation (Figure 1c). The conformation of Ser65 facing His64 had a X_1 angle of −176.3° while the other conformation facing away from His64 was 70.8°. Of additional interest was that the proton-shuttle residue His64 in the CA IX mimic showed a dual conformation similar to that previously described for CA II (*35*). This implies that the proton shuttling differences were most likely due to residues outside of the cavity.

All the inhibitor complex structures for both CA II and the CA IX mimic share the same general well characterized sulfonamide binding profile. The N(1) group coordinates to the zinc with a hydrogen bond distance of approximately 2.0 Å and interacts with the nitrogens of His94, His96, and His119 at 3.3−3.6 Å, as well as Thr199 between 2.8−3.0 Å. One oxygen of the sulfonamide group binds to Thr199 at a distance of 3.0−3.2 Å. The other oxygen binds His94 at 3.5 Å, His119 at 3.6 Å, and Zn^{2+} at 3.0−3.1 Å. The sulfonamide sulfur binds Zn^{2+} with a distance of 3.0 Å. There is a Van der Waals interaction with His94 at a distance of 3.2−3.4 Å as well as numerous weak hydrophobic contacts with residues Trp209, His119, His96, His94, Val121, and Leu198 (listed in Table 5).

In AZM, the two nitrogens of the thiadiazole ring form hydrogen bonds with Thr200 at distances of 2.9−3.0 Å and 3.1 Å, respectively. It also forms weak hydrophobic contacts with residues His119, His96, Val143 and Val121 in both CA II and the CA IX mimic (Figure 2b). The CA II AZM structure contains an additional hydrogen bond with Gln92 with changes to the conformation of the residue and leads

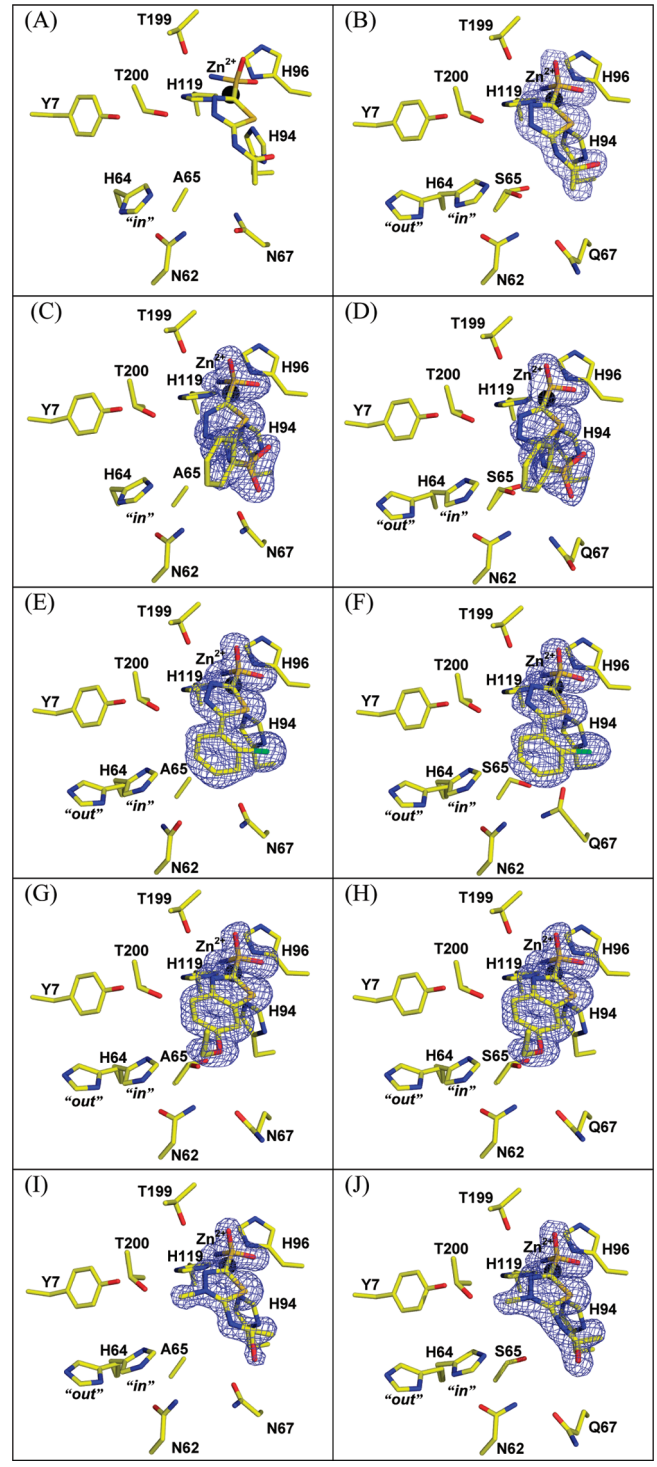

FIGURE 2: Crystal structures of the active site of CA II and CA IX mimic in complex with inhibitors (A) CA II with AZM, (B) CA IX mimic with AZM, (C) CA II with BZM, (D) CA IX mimic with BZM, (E) CA II with CHL, (F) CA IX mimic with CHL, (G) CA II with EZM, (H) CA IX mimic with EZM, (I) CA II with MZM, and (J) CA IX mimic with MZM. The Zn^{2+} atom is labeled and shown as a black sphere; side chain residues are labeled and atom coloring is as follows: carbon (yellow), oxygen (red), nitrogen (blue), sulfur (orange), and chlorine (green). The blue 2Fo−Fc electron density maps shown are contoured at 1.5σ. Figure generated in PyMOL (*43*).

Table 5: Inhibitor−Protein Interactions (Å)

interactions found in all structures	interactions found in individual drugs	interactions in individual structures
N1 HB[a]: His96 (3.3−3.5), Thr199 (2.8−3.0), ZN^{2+} (1.9−2.3), His94 (3.3−3.5), His119 (3.3−3.6) **O2/O4 HB:** His94 (3.5), Zn^{2+} (3.0−3.1), His119 (3.6) **O1/O3 HB:** Thr199 (3.0−3.2) **S1/S3 HB:** Zn^{2+} (3.0−3.1) **HC[b]:** His94 (3.2−3.4) **wHC[c]:** Trp209 (3.6−3.9), His119 (4.0), His119 (3.9) *[except CA II MZM]*, His96 (3.7−4.0) *[except CA II MZM]*, Val121 (3.7−3.9, 3.8−4.0), His94 (3.8−4.0, 3.8−4.0, 3.8−4.0), Leu198 (3.6−3.7, 3.7−3.8, 3.8−3.9, 3.9, 3.7−4.0, 3.7−4.0)	**AZM:** **N3 HB:** Thr200 (2.9−3.0) **N2 HB:** Thr200 (3.1) **wHC:** His119 (3.8−3.9, 3.9), His96 (3.8), Val143 (4.0), Val121 (3.7−3.8, 3.8−3.9) **BZM:** **N3 HB:** Thr200 (2.9−3.1) **O2 HB:** Gln92 (3.3−3.4) **HC:** Phe131 (3.3), Leu198 (3.3) **wHC:** His96 (3.7−3.8), His119 (3.9), Val143 (4.0), Val121 (3.9), Phe131 (3.5−3.6, 3.7−3.8, 3.7−3.9,3.8−3.9, 4.0) **CHL:** **O2 HB:** His119 (3.6) **N2 HB:** Thr199 (3.5−3.6), Thr200 (3.4−3.5) **N1 HB:** Thr200 (3.0−3.1) **HC:** Leu198 (3.4−3.5), Trp209 (3.5) **wHC:** His96 (3.8), His119 (3.8, 3.9), Thr199 (4.0), Phe131 (3.8, 3.8, 3.8−3.9), Leu198 (3.5−3.6) **EZM:** **N2 HB:** Thr200 (3.2−3.4) **HC:** Leu198 (3.4, 3.5−3.6), Thr200 (2.9−3.0, 3.4−3.5) **wHC:** Trp209 (4.0), Val143 (4.0), His119 (3.8, 3.9), His96 (3.8), Thr199 (3.9), Thr200 (3.7), Pro201 (3.7, 3.7−3.8), Leu198 (3.9−4.0), Pro202 (3.9) **MZM:** **O1 HB:** His119 (3.4−3.6) **HC:** Thr200 (3.0−3.1), Pro201 (3.5−3.6) **wHC:** Thr200 (3.8), Phe131 (3.6, 3.7, 3.8)	**CA II AZM[d]:** **O3 HB:** Gln92 (3.2) **HC:** Gln92 (3.2), Val121 (3.5), Phe131 (3.5, 3.4) **wHC:** Gln92 (3.6, 4.0, 3.8), Phe131 (3.6, 3.7), Leu198 (4.0) **CA IX mimic AZM:** **O1 HB:** Thr199 (3.6) **wHC:** Trp209 (4.0), Gln92 (3.8, 4.0), Phe131 (3.7, 3.8, 3.8, 3.8) **CA II BZM:** **N2 HB:** Thr200 (3.2) **N1 HB:** Gln92 (3.6) **wHC:** Gln92 (3.9), Phe131(4.0), Leu198 (4.0) **CA IX mimic BZM:** **N2 HB:** Thr200 (2.9) **wHC:** His94 (3.9), Thr200 (4.0, 4.0), Phe131 (3.9), Val135 (3.9) **CA II CHL:** **wHC:** Leu198 (3.6, 3.6, 3.7, 3.7, 3.9) **CA IX CHL:** **CL1 HB:** Gln92 (3.5) **wHC:** Val121 (4.0), Leu198 (3.8, 3.9, 3.9, 4.0) **CA II EZM:** **wHC:** Thr200 (4.0), Phe131 (4.0), Leu198 (4.0) **CA IX mimic EZM:** **wHC:** Pro202 (3.8) **CA II MZM:** **HC:** Gln92 (3.5) **wHC:** Val121 (4.0), Gln92 (3.8, 4.0, 4.0) **CA IX MZM:** **HC:** Trp209 (3.5), Val121 (3.5), Gln92 (3.4, 3.4) **wHC:** His96 (4.0), His119 (3.9, 4.0), Thr199 (3.9), Val121 (3.9, 4.0), Leu198 (3.9, 3.9), Gln92 (3.7, 3.8, 3.9)

[a] HB = hydrogen bond (2.0−3.6 Å). [b] Hydrophobic contact (3.0−3.6 Å). [c] wHC = weak hydrophobic contacts (3.6−4.0 Å). [d] CA II AZM coordinates provided by Dr. Arthur Robbins (personal communication).

to more hydrophobic interactions with Val121 and Phe131, and weakly with Leu198. For the CA IX mimic AZM, there was an additional hydrogen bond with Thr199, which created several weak hydrophobic contacts with Trp209, Gln92, and Phe131. In both structures of BZM, the O(2) of the sulfonamide hydrogen bonds with the nitrogen of Gln92 at a distance of 3.3−3.4 Å, N(3) hydrogen bonds with Thr200 at 2.9−3.1 Å, and more hydrophobic contacts are made with Leu198 and Phe131, as well as several weak hydrophobic interactions (Figure 2c). The CA II BZM structure has two additional hydrogen bonds, one to Thr200 at 3.2 Å and the other to Gln92 at 3.6 Å. In the CA IX mimic complexed with BZM, there is a 2.9 Å hydrogen bond of the N(2) to Thr200. There are also weak hydrophobic contacts seen with residues His94, Thr200, Phe131 and Val135 (Figure 2d). EZM has nearly identical interactions with both CA II and CA IX mimic, which consists of the N(2) hydrogen bonding to Thr200 at 3.2−3.4 Å and of hydrophobic contacts including Thr200, Leu198, Trp209, His96, His119, Thr199, Pro201, Pro202, and Val143 (Figure 2g,h). There are only a few weak Van der Waals interactions different between the two. MZM forms an additional hydrogen bond between O(1) and His119 at a distance of 3.4−3.5 Å and hydrophobic contacts with Thr200, Pro201, and Phe131 in both CA II and CA IX mimic. Most of the difference between CA II and the CA IX mimic bound to MZM are in weak hydrophobic interactions (Figure 2i,j).

In the case of CHL, both structures show O(2) hydrogen bonding to His119 at 3.6 Å, N(2) binding Thr199 at 3.5−3.6 Å and Thr200 at 3.4−3.5 Å, and N(1) hydrogen bonding to Thr200 at a distance of 3.0−3.1 Å. There are also several Van der Waals contacts with residues Leu198, Trp209, His96, His119, Thr199, and Phe131. The structure of CA II CHL show several new weak hydrophobic interactions (Figure 2e). However, in the crystal structure of CA IX mimic in complex with CHL, the chlorine hydrogen bonds with Gln92; this pulls residue Gln67 into the active site and fixes Ser65 into one conformation oriented toward the His64 with a X_1 angle of 111.4° (Figure 2f and Figure 3a,b).

When the drugs are superimposed on one another, the similarities and differences of binding become apparent (Figure 3c−f). The sulfonamide groups are in nearly superimposible orientations. For the most part, the thiadiazole ring and hydrophobic tail are locked into a planar geometry with two exceptions. In EZM the thiadiazole ring is rotated out slightly, probably due to the additional conjugated ring, and the ethoxy group lies nearly perpendicular to the regular plane. In BZM, the thiadiazole ring

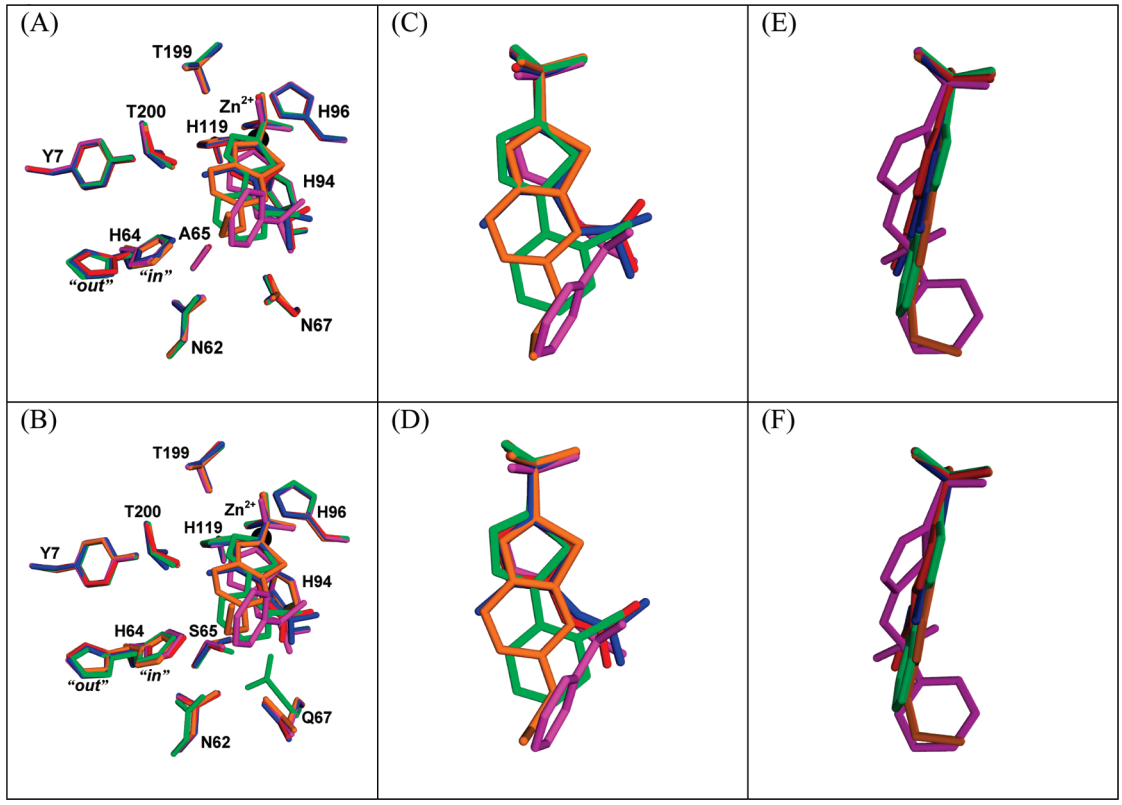

FIGURE 3: Superposition of all five drug complexes in crystal structures. (A) Active sites of CA II complexes. (B) Active sites of CA IX mimic complexes. AZM (red), BZM (magenta), CHL (green), EZM (orange), MZM (blue), Zn^{2+} (black sphere). (C), (D) Superposition of all five drugs in CA II and CA IX mimic, respectively. (E), (F) Superposition of all five drugs in CA II and CA IX mimic, respectively, rotated 90° from previous view. Figure generated in PyMOL (*43*).

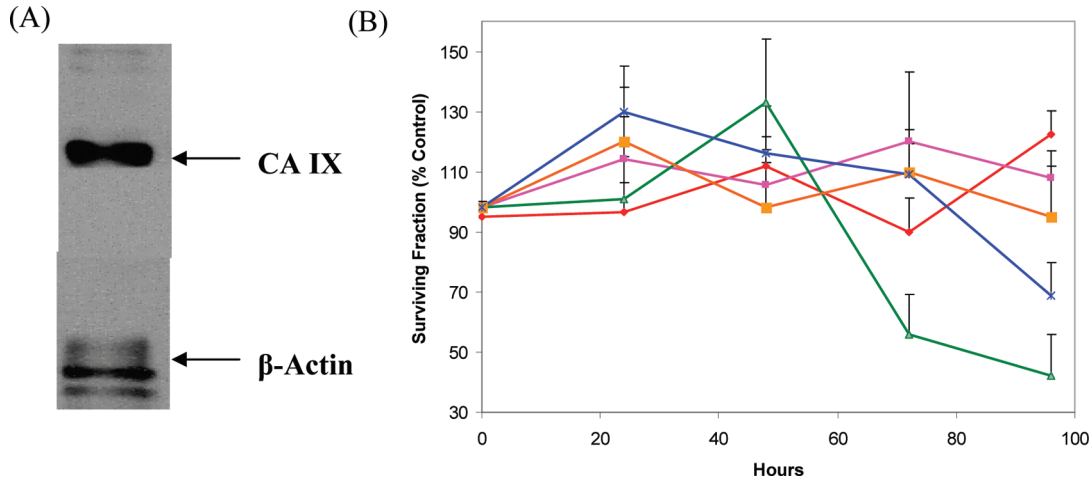

FIGURE 4: Cell proliferation analysis in PC-3-*Bcl*-2 prostate cancer cell lines. (A) Western blot analysis verifying the expression of CA IX by the PC-3-*Bcl*-2 cells. (B) PC-3-*Bcl*-2 cells were treated with one of the following inhibitors: AZM (red), BZM (magenta), CHL (green), EZM (orange), or MZM (blue) at 0.1 mM for 96 h and then subjected to an MTT assay. *X*-axis, exposure time (h); *Y*-axis, % surviving fraction compared to mock (DMSO only). Only compounds CHL and MZM demonstrated reduced proliferation compared to the mock (43% and 68%, respectively). Each assay was performed in triplicate, and the mean for all three experiments was calculated. Crystal violet exclusion test confirmed the above MTT results (i.e., decrease proliferation) were associated with an increase cell death.

is rotated significantly out of the plane and the phenylsulfonyl is rotated nearly 90° as compared to the hydrophobic tails of the AZM, CHL, and MZM and aligning with the ethoxy of EZM.

PC-3-Bcl-2 Western Blot and Cytotoxicity Assay. A Western blot was performed on untreated PC-3-*Bcl*-2 cells to verify the expression of CA IX in this cancer cell line (Figure 4a). To determine the effects of carbonic anhydrase inhibitors on cell proliferation and viability, PC-3-*Bcl*-2 prostate cancer cell lines were treated for 96 h with the carbonic anhydrase inhibitors (at concentrations ranging from 0 to 10 0000 nM), control or mock. Cellular proliferation is depicted at 0.1 mM for all agents (Figure 4b). AZM, BZM, and EZM even at higher doses had no cytotoxic effects. However, MZM at 0.01 and 0.1 mM demonstrated significant inhibition of proliferation and viability compared to the control (29% and 32% inhibition respectively, $p < 0.01$). For inhibitor CHL, significant reduction in cellular prolifera-

tion and viability was evident only at 0.1 mM (57% inhibition, $p < 0.01$). It is important to note that these values are consistent with those previously published for in vitro studies of sulfonamides in cancer cell lines (*3, 40*).

DISCUSSION

This work describes the kinetic and structural characterization of a CA IX mimic. Translating the knowledge derived from this mimic to in vitro studies has identified potential drugs for cancers overexpressing CA IX.

The kinetic characterization of the CA IX mimic demonstrates that the two amino acid mutations in CA II to CA IX do imitate CA IX in terms of chemistry at the active-site zinc ion. The values of k_{cat}/K_m for the CA IX mimic are similar to those reported for the CA domain of CA IX in Wingo et al. and in Hilvo et al. (*17, 18*). However, these values are lower than those reported for the CA domain with the N-terminal proteoglycan domain in Hilvo et al. (*18*). The k_{cat}/K_m of both the CA IX mimic and CA IX exhibit a 2-fold decrease as compared to CA II which is probably due to a change in hydrophobic properties in the active site caused by the change from the hydrophobic alanine at position 65 to the polar serine residue. In terms of chemistry at His64, however, the kinetic properties of the CA IX mimic are still much like those of CA II. This is likely because there is no significant change in the active-site residues that coordinate the waters in the active-site cavity. This means there is possibly another, non-active-site residue that causes the difference in proton transfer between CA II and CA IX. Further investigation into several theoretical proton shuttling residues identified by molecular dynamics reveal two mutations that might improve the kinetics (*41, 42*). The first is Glu69, a Thr in CA IX, and Lys170, which is a Glu. However, despite the difference in proton transfer rates between the CA IX mimic and CA IX, the kinetic profile of the CA II double mutant seems like a good model for inhibition of CA IX in the active-site cavity.

To assess the viability of the CA IX mimic as an analog of wild-type CA IX, the K_i values have been compared to CA II with the classic sulfonamides. The CA IX mimic values correspond preferentially to wild-type CA IX, lending credence to use the mimic as a model for CA IX isozyme specificity. However, the CA IX mimic is not perfect, as demonstrated by the slight disparity in K_i values between CA IX mimic and wild-type. The differences fall within statistical variation, and given the difficulties in expressing wild-type CA IX, the mimic may provide an opportunity to prescreen possible drugs or as a model for rational drug design.

Recently, a study was published characterizing biochemically the extracellular domains of native CA IX. Among the conclusions of this paper was the identification of both dimeric and monomeric forms of CA IX, in the ratio of 60% to 34%, respectively (*18*). Homology modeling of CA IX revealed that the location of the intermolecular disulfide is located on the opposite side of the enzyme, away from the active site. From this information, it was concluded that the dimeric state probably does not affect catalytic activity and, as a result, the monomeric CA IX mimic is still a satisfactory model for CA IX inhibition.

In assuming that the CA IX mimic is an adequate analog, the study reveals valuable information regarding the isozyme specificity of classical sulfonamides. The kinetics and crystal structures reveal an interesting story. In the case of AZM, the K_i value is lowered by a factor of 2 in the CA IX mimic, making it a better inhibitor of the mutant than CA II. This could be due to the conformational change of Gln92 in the structure of CA IX mimic as compared to CA II; however, the in vitro studies show AZM has no cytotoxic effect on the PC-3-*Bcl*-2 cells. As a result, our study indicates that AZM may not be the most effective agent for this purpose.

BZM and MZM show few differences kinetically or structurally, making them less likely to be preferentially effective against the CA IX found in cancer cells. This being said, MZM did show cytotoxic effects against PC-3-*Bcl*-2 cells, which indicates that it cannot be excluded from the list of possible anticancer therapies. EZM cannot be adequately assessed kinetically due to its subnanomolar K_i, and there are few clues structurally as to its isozyme specificity other than increased surface area binding (unpublished data). Until a more sensitive test of kinetics is developed, its potency presents a risk as a cancer treatment due to the high likelihood of inhibiting CA II.

The results of this study suggest that CHL has the most potential for therapeutics. Comparing the structures of CA II versus the CA IX mimic, the chlorine in CHL hydrogen binds to Gln92 in the mimic and not in CA II. This may be the reason for the conformational change of Gln67 and the locking of Ser65 into one position oriented toward His64. Kinetically, the K_i value is the lowest in the CA IX mimic, excluding EZM. The increased inhibition is possibly due to the aforementioned Gln67, which is a mutated active-site residue being pulled into a locked down conformation by Gln92 then hydrogen bonding to the other mutant residue Ser65. This binding mode is different from the sulfonamides in CA II, which typically bind in a "lock and key" mechanism, which does not induce conformational changes. Also, CHL is the only structure with a bulky chloride present and halides, such as chlorine, are known to affect the hydrostatics of the surrounding environment. The hydrostatic change of the environment is causing this locked-down effect improving the inhibition and selectivity of CHL. This evidence is supported by the cytotoxicity assay, which shows CHL not only impedes propagation of PC-3-*Bcl*-2 cells but also induces cell death.

In conclusion, we have developed an effective surrogate of CA IX for use in high-throughput kinetic and structural screenings. The fact that the crystallographic analysis and kinetic studies of the CA IX mimic correlated to the cytotoxicity assay only serves to reinforce this claim. Of the five drugs studied, AZM, MZM, and CHL were identified as potential anticancer drugs, alone or in conjunction with traditional chemotherapy. Further, in vitro and in vivo studies are needed to confirm this assertion, as well as an investigation into the disparity between K_i values and growth inhibition curves in vivo. The CA IX mimic also presents a unique opportunity for quick screening of novel CA IX inhibitors.

REFERENCES

1. Krishnamurthy, V. M., Kaufman, G. K., Urbach, A. R., Gitlin, I., Gudiksen, K. L., Weibel, D. B., and Whitesides, G. M. (2008)

Carbonic anhydrase as a model for biophysical and physical-organic studies of proteins and protein-ligand binding. *Chem. Rev. 108*, 946–1051.
2. Maren, T. H., and Conroy, C. W. (1993) A new class of carbonic anhydrase inhibitor. *J. Biol. Chem. 268*, 26233–26239.
3. Supuran, C. T., Briganti, F., Tilli, S., Chegwidden, W. R., and Scozzafava, A. (2001) Carbonic anhydrase inhibitors: sulfonamides as antitumor agents? *Bioorg. Med. Chem. 9*, 703–714.
4. Supuran, C. T., Casini, A., and Scozzafava, A. (2003) Protease inhibitors of the sulfonamide type: anticancer, antiinflammatory, and antiviral agents. *Med. Res. Rev. 23*, 535–558.
5. Pastorekova, S., Parkkila, S., Pastorek, J., and Supuran, C. T. (2004) Carbonic anhydrases: current state of the art, therapeutic applications and future prospects. *J. Enzyme Inhib. Med. Chem. 19*, 199–229.
6. Wilkinson, B. L., Bornaghi, L. F., Houston, T. A., Innocenti, A., Vullo, D., Supuran, C. T., and Poulsen, S. A. (2007) Inhibition of membrane-associated carbonic anhydrase isozymes IX, XII and XIV with a library of glycoconjugate benzenesulfonamides. *Bioorg. Med. Chem. Lett. 17*, 987–992.
7. Thiry, A., Dogne, J. M., Masereel, B., and Supuran, C. T. (2006) Targeting tumor-associated carbonic anhydrase IX in cancer therapy. *Trends Pharmacol. Sci. 27*, 566–573.
8. Potter, C. P., and Harris, A. L. (2003) Diagnostic, prognostic and therapeutic implications of carbonic anhydrases in cancer. *Br. J. Cancer 89*, 2–7.
9. Gullino, P. M., Grantham, F. H., and Smith, S. H. (1965) The Interstitial Water Space of Tumors. *Cancer Res. 25*, 727–731.
10. Gullino, P. M., Grantham, F. H., Smith, S. H., and Haggerty, A. C. (1965) Modifications of the acid-base status of the internal milieu of tumors. *J. Natl. Cancer Inst. 34*, 857–869.
11. Helmlinger, G., Sckell, A., Dellian, M., Forbes, N. S., and Jain, R. K. (2002) Acid production in glycolysis-impaired tumors provides new insights into tumor metabolism. *Clin. Cancer Res. 8*, 1284–1291.
12. Svastova, E., Zilka, N., Zat'ovicova, M., Gibadulinova, A., Ciampor, F., Pastorek, J., and Pastorekova, S. (2003) Carbonic anhydrase IX reduces E-cadherin-mediated adhesion of MDCK cells via interaction with beta-catenin. *Exp. Cell Res. 290*, 332–345.
13. Teicher, B. A., Liu, S. D., Liu, J. T., Holden, S. A., and Herman, T. S. (1993) A carbonic anhydrase inhibitor as a potential modulator of cancer therapies. *Anticancer Res. 13*, 1549–1556.
14. Parkkila, S., Rajaniemi, H., Parkkila, A. K., Kivela, J., Waheed, A., Pastorekova, S., Pastorek, J., and Sly, W. S. (2000) Carbonic anhydrase inhibitor suppresses invasion of renal cancer cells in vitro. *Proc. Natl. Acad. Sci. U.S.A. 97*, 2220–2224.
15. Xiang, Y., Ma, B., Li, T., Yu, H. M., and Li, X. J. (2002) Acetazolamide suppresses tumor metastasis and related protein expression in mice bearing Lewis lung carcinoma. *Acta Pharmacol. Sin. 23*, 745–751.
16. Supuran, C., and Scozzafava, A. (2002) Applications of carbonic anhydrase inhibitors and activators in therapy. *Expert Opin. Ther. Pat. 12*, 217–241.
17. Wingo, T., Tu, C., Laipis, P. J., and Silverman, D. N. (2001) The catalytic properties of human carbonic anhydrase IX. *Biochem. Biophys. Res. Commun. 288*, 666–669.
18. Hilvo, M., Baranauskiene, L., Salzano, A. M., Scaloni, A., Matulis, D., Innocenti, A., Scozzafava, A., Monti, S. M., Di Fiore, A., De Simone, G., Lindfors, M., Janis, J., Valjakka, J., Pastorekova, S., Pastorek, J., Kulomaa, M. S., Nordlund, H. R., Supuran, C. T., and Parkkila, S. (2008) Biochemical characterization of CA IX: one of the most active carbonic anhydrase isozymes. *J. Biol. Chem.*
19. Thompson, J. D., Higgins, D. G., and Gibson, T. J. (1994) CLUSTAL W: improving the sensitivity of progressive multiple sequence alignment through sequence weighting, position-specific gap penalties and weight matrix choice. *Nucleic Acids Res. 22*, 4673–4680.
20. Fisher, S. Z., Maupin, C. M., Budayova-Spano, M., Govindasamy, L., Tu, C., Agbandje-McKenna, M., Silverman, D. N., Voth, G. A., and McKenna, R. (2007) Atomic crystal and molecular dynamics simulation structures of human carbonic anhydrase II: insights into the proton transfer mechanism. *Biochemistry 46*, 2930–2937.
21. Schwede, T., Kopp, J., Guex, N., and Peitsch, M. C. (2003) SWISS-MODEL: An automated protein homology-modeling server. *Nucleic Acids Res. 31*, 3381–3385.
22. Emsley, P., and Cowtan, K. (2004) Coot: model-building tools for molecular graphics. *Acta Crystallogr., Sect. D: Biol. Crystallogr. 60*, 2126–2132.
23. Gillam, S., and Smith, M. (1979) Site-specific mutagenesis using synthetic oligodeoxyribonucleotide primers: II. In vitro selection of mutant DNA. *Gene 8*, 99–106.
24. Gillam, S., and Smith, M. (1979) Site-specific mutagenesis using synthetic oligodeoxyribonucleotide primers: I. Optimum conditions and minimum ologodeoxyribonucleotide length. *Gene 8*, 81–97.
25. Davanloo, P., Rosenberg, A. H., Dunn, J. J., and Studier, F. W. (1984) Cloning and expression of the gene for bacteriophage T7 RNA polymerase. *Proc. Natl. Acad. Sci. U.S.A. 81*, 2035–2039.
26. Studier, F. W., and Moffatt, B. A. (1986) Use of bacteriophage T7 RNA polymerase to direct selective high-level expression of cloned genes. *J. Mol. Biol. 189*, 113–130.
27. Khalifah, R. G. (1977) Histidine-200 alters inhibitor binding in human carbonic anhydrase B. A carbon-13 nuclear magnetic resonance identification. *Biochemistry 16*, 2236–2240.
28. McPherson, A. (1982) *Preparation and Analysis of Protein Crystals*, John Wiley and Sons, New York.
29. Otwinowski, Z., and Minor, W. (1997) *Processing of X-ray Diffraction Data Collected in Oscillation Mode*, Vol. 276, Yale University, New Haven, CT.
30. Brunger, A. T., Adams, P. D., Clore, G. M., DeLano, W. L., Gros, P., Grosse-Kunstleve, R. W., Jiang, J. S., Kuszewski, J., Nilges, M., Pannu, N. S., Read, R. J., Rice, L. M., Simonson, T., and Warren, G. L. (1998) Crystallography & NMR system: A new software suite for macromolecular structure determination. *Acta Crystallogr., Sect. D: Biol. Crystallogr. 54*, 905–921.
31. Schuttelkopf, A. W., and van Aalten, D. M. (2004) PRODRG: a tool for high-throughput crystallography of protein-ligand complexes. *Acta Crystallogr., Sect. D: Biol. Crystallogr. 60*, 1355–1363.
32. Sheldrick, G. M. (2008) A short history of SHELX. *Acta Crystallogr., Sect. A: Found. Crystallogr. 64*, 112–122.
33. Laskowski, R. A., Moss, D. S., and Thornton, J. M. (1993) Main-chain bond lengths and bond angles in protein structures. *J. Mol. Biol. 231*, 1049–1067.
34. Silverman, D. N. (1982) Carbonic anhydrase: oxygen-18 exchange catalyzed by an enzyme with rate-contributing proton-transfer steps. *Methods Enzymol. 87*, 732–752.
35. Fisher, Z., Hernandez Prada, J. A., Tu, C., Duda, D., Yoshioka, C., An, H., Govindasamy, L., Silverman, D. N., and McKenna, R. (2005) Structural and kinetic characterization of active-site histidine as a proton shuttle in catalysis by human carbonic anhydrase II. *Biochemistry 44*, 1097–1105.
36. Segel, I. (1975) *Enzyme Kinetics: Behavior and Analysis of Rapid Equilibrium and Steady-State Enzyme Systems*, Wiley-Interscience, New York.
37. Anai, S., Shiverick, K., Medrano, T., Nakamura, K., Goodison, S., Brown, B. D., and Rosser, C. J. (2007) Downregulation of BCL-2 induces downregulation of carbonic anhydrase IX, vascular endothelial growth factor, and pAkt and induces radiation sensitization. *Urology 70*, 832–837.
38. Goodison, S., Nakamura, K., Iczkowski, K. A., Anai, S., Boehlein, S. K., and Rosser, C. J. (2007) Exogenous mycoplasmal p37 protein alters gene expression, growth and morphology of prostate cancer cells. *Cytogenet. Genome Res. 118*, 204–213.
39. Silverman, D. N., and Tu, C. K. (1976) Carbonic anhydrase catalyzed hydration studied by 13C and 18O labeling of carbon dioxide. *J. Am. Chem. Soc. 98*, 978–984.
40. Svastova, E., Hulikova, A., Rafajova, M., Zat'ovicova, M., Gibadulinova, A., Casini, A., Cecchi, A., Scozzafava, A., Supuran, C. T., Pastorek, J., and Pastorekova, S. (2004) Hypoxia activates the capacity of tumor-associated carbonic anhydrase IX to acidify extracellular pH. *FEBS Lett. 577*, 439–445.
41. Riccardi, D., Konig, P., Guo, H., and Cui, Q. (2008) Proton transfer in carbonic anhydrase is controlled by electrostatics rather than the orientation of the acceptor. *Biochemistry 47*, 2369–2378.
42. Roy, A., and Taraphder, S. (2007) Identification of proton-transfer pathways in human carbonic anhydrase II. *J. Phys. Chem. B 111*, 10563–10576.
43. DeLano, W. L. (2002), Delano Scientific, Palo Alto, CA.

BI802035F